International Journal of Heat and Mass Transfer 130 (2019) 857–861

Contents lists available at ScienceDirect

International Journal of Heat and Mass Transfer

journal homepage: www.elsevier.com/locate/ijhmt

Technical Note

Lattice Boltzmann modeling and experimental study of water droplet spreading on wedge-shaped pattern surface

Xiaoyu Zhang [a], Mengyu Huang [a], Qian Ji [b,*], Xiaobing Luo [a,*]

[a] State Key Laboratory of Coal Combustion, School of Energy and Power Engineering, Huazhong University of Science and Technology, Wuhan 430074, China
[b] School of Mechanical Science & Engineering, Huazhong University of Science and Technology, Wuhan 430074, China

ARTICLE INFO

Article history:
Received 3 May 2018
Received in revised form 18 October 2018
Accepted 3 November 2018

Keywords:
Wedge-shaped pattern surface
Lattice Boltzmann method
Hydrophilic and hydrophobic regions

ABSTRACT

Water droplet on wedge-shaped pattern surface with hydrophilic and hydrophobic regions can spread spontaneously in a specific direction. In this study, we investigated the mechanism of the surface tension-driven spontaneous drop spreading behaviors by the lattice Boltzmann modeling and experimental validation. Based on the Shan-Chen (SC) type multicomponent multiphase model with an algorithm for relatively accurate contact angle measuring, we simulated four cases with various vertex angles (ψ = 15°, 20°, 28°, 35°) of wedge-shaped pattern. After then, such surfaces were fabricated and corresponding experiments were conducted. The time dependence of the droplet move distance was characterized in both the simulations and experiments with average deviation within 6.11%. Related force contour and vector analyses were presented to discuss the driving mechanism. This study is expected to shed light on the physical exploration and provide insightful hints to better tune and control the directional spreading of the surface tension-driven droplet.

1. Introduction

Droplet wetting and spreading on solid surface is important to many industrial processes in a variety of applications such as ventilation, air conditioning and electronics thermal management [1–7]. For example, the condensation on the hydrophilic metal surface of a heat exchanger will form a thin water layer, which acts as a thermal barrier to reduce the heat exchange efficiency [8]. By modifying the metal surface to a patterned surface with alternating hydrophilic and hydrophobic regions, the condensed droplets will spontaneously spread from the hydrophobic region to the hydrophilic region directionally, which greatly drains the droplets to avoid the formation of large-area water layer and improve the heat exchange efficiency [9,10]. Quite a lot of works were reported on studying such patterned surfaces with *stripe* [11], circle [9], wedge-shaped [12] and Y-shaped [13] patterns via surface fabrication and simulation. Among these patterns, the wedge-shaped pattern creates a surface tension gradient that makes it easy to manipulate water droplet spreading towards a desired direction. Alheshibri et al. [14] has proposed a reliable method for fabricating a wedge-shaped pattern on an Al/Cu surface with experimental validation. However, to further extend this surface treatment method, it is necessary to well understand the fundamental mechanism and then do the parameter optimization. Due to the limited cases in experiments, such mechanism remained unaccounted yet [14]. Comparably, numerical modeling is an powerful and flexible tool to handle this issue. Preferably, the lattice Boltzmann method (LBM) based on mesoscopic kinetic equations is a convenient technique for simulating multi-phase fluid flows, which has recently become popular in the study of droplet wetting and spreading [15–17].

In view of the status quo, we adopt the LBM to simulate water droplet spreading on wedge-shaped pattern surface with vertex angles of 15°, 20°, 28°, 35°. After then, the corresponding surfaces with the same vertex angles were fabricated and experimentally studied. The droplet move distance in the simulation was compared with that in the experiment to verify the accuracy of modeling. In addition, the driving force contour and vector on the droplet surface were analyzed to discuss the mechanism in the spreading process.

2. Lattice Boltzmann simulations

Here we used Shan-Chen (SC) type multicomponent multiphase model on account of an algorithm for relatively accurate contact angle measuring [18,19], which is widely used in droplet spreading process for its conceptual simplicity and high computational efficiency. Here we used D3Q19 model. In SC model, the particle distribution function satisfies the following LB equation:

* Corresponding authors.
E-mail addresses: jiqian@mail.hust.edu.cn (Q. Ji), luoxb@hust.edu.cn (X. Luo).

https://doi.org/10.1016/j.ijheatmasstransfer.2018.11.013
0017-9310/

$$f_{\sigma i}(x+e_i dt, t+dt) - f_{\sigma i}(x,t) = -\frac{1}{\tau_\sigma}\left[f_{\sigma i}(x,t) - f^{eq}_{\sigma i}(x,t)\right] \quad (1)$$

where $f_{\sigma i}(x,t)$ is the particle distribution function of component σ (the opposite component is $\overline{\sigma}$) in the i^{th} velocity direction at site x and time step t. τ_σ is the relaxation time, and e_i is the discrete velocities. $f^{eq}_{\sigma i}(x,t)$ is the equilibrium distribution function calculated by:

$$f^{eq}_{\sigma i} = \omega_i \rho \left[1 + \frac{\mathbf{e_i}\cdot\mathbf{u}}{c_s^2} + \frac{(\mathbf{e_i}\cdot\mathbf{u})^2}{2c_s^4} - \frac{\mathbf{u}^2}{2c_s^2}\right] \quad (2)$$

Here c_s is the lattice sound speed and ω_i is the weighting coefficient. The density and macroscopic velocity of the component σ at a lattice site are given by:

$$\rho_\sigma(x,t) = \sum_i f^{eq}_{\sigma i} \quad (3)$$

$$\mathbf{u} = \mathbf{u}' + \frac{\tau_\sigma F_\sigma}{\rho_\sigma} \quad (4)$$

with

$$\mathbf{u}' = \sum_\sigma \left(\sum_i \frac{f_{\sigma i} e_i}{\tau_\sigma}\right) \Big/ \sum_\sigma \frac{\rho_\sigma}{\tau_\sigma} \quad (5)$$

In Eq. (4), $F_\sigma = F_{c,\sigma} + F_{ads,\sigma}$ is the force acting on the component σ. The gravitational force is ignored, since the volumes used in the experiment are small enough to be neglected. Here $F_{c,\sigma}$ is the cohesion force that determines the surface tension:

$$\boldsymbol{F}_{c,\sigma} = -G_c \rho_\sigma(x,t) \sum_i \omega_i \rho_{\bar{\sigma}}(x + \mathbf{e_i}\Delta t, t)\mathbf{e_i} \quad (6)$$

Each site is occupied by two components, where the minor component is thought of as dissolved within the dominant component. Thus the densities are complementary ($\rho_\sigma + \rho_{\bar{\sigma}} = \rho_i$, ρ_i is the constant initial density). G_c is a parameter that determines the strength of the cohesion force. A too large G_c will make two phases immiscible, while a too low G_c will cause two phases to mix into one single phase. Huang et al. [19] found that the model is more stable when $1.6 < G_c(\rho_\sigma + \rho_{\bar{\sigma}}) < 2.0$, particularly when the expression equals 1.8 and G_c equals 0.87. Here we chose the same values, so ρ_i equals 2.06.

$F_{ads,\sigma}$ represents the adhesion force between the fluid and solid:

$$\boldsymbol{F}_{ads,\sigma}(x) = -G_{ads,\sigma}\rho_\sigma(x,t) \sum_i \omega_i s(x + \mathbf{e_i}\Delta t)\mathbf{e_i} \quad (7)$$

where $G_{ads,\sigma}$ is the interaction strength between the component and the solid wall. Here s equals 0 or 1 which represents fluid or solid site. According to Huang et al. [19], the equation below provides a relatively accurate contact angle measurement:

$$\cos\theta_1 = \frac{G_{ads,2} - G_{ads,1}}{G_c(\rho_1 - \rho_2)/2} \quad (8)$$

where ρ_1 and ρ_2 are the dominant density and associate dissolved density, respectively. According to Huang et al. [19], the simulation is most stable when the adhesive constants of two fluid components are opposite to each other, i.e., $G_{ads,2} = -G_{ads,1}$.

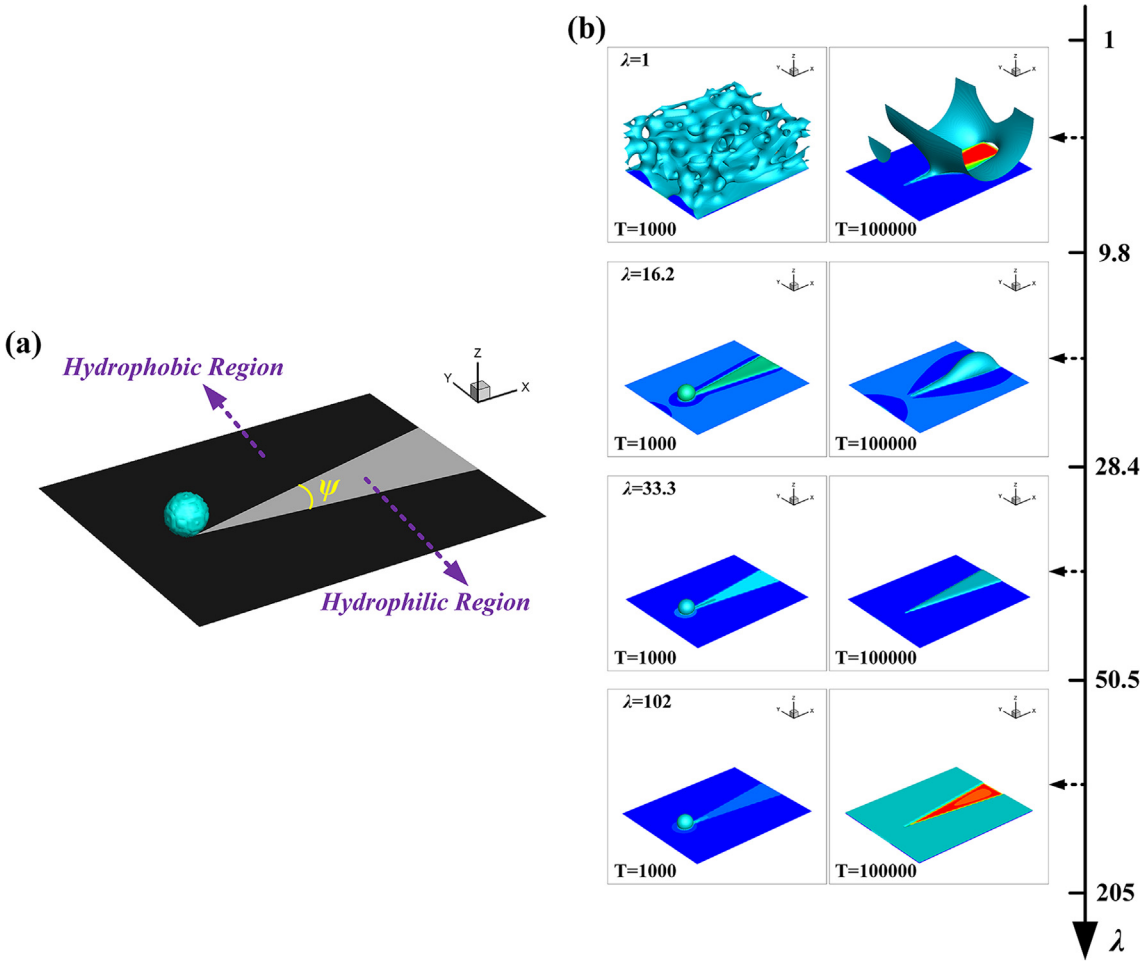

Fig. 1. (a) Simulation set-up. (b) Simulated droplet spreading morphology in the 15° vertex angle case under different density ratio λ at time step of T = 1000 and 100,000.

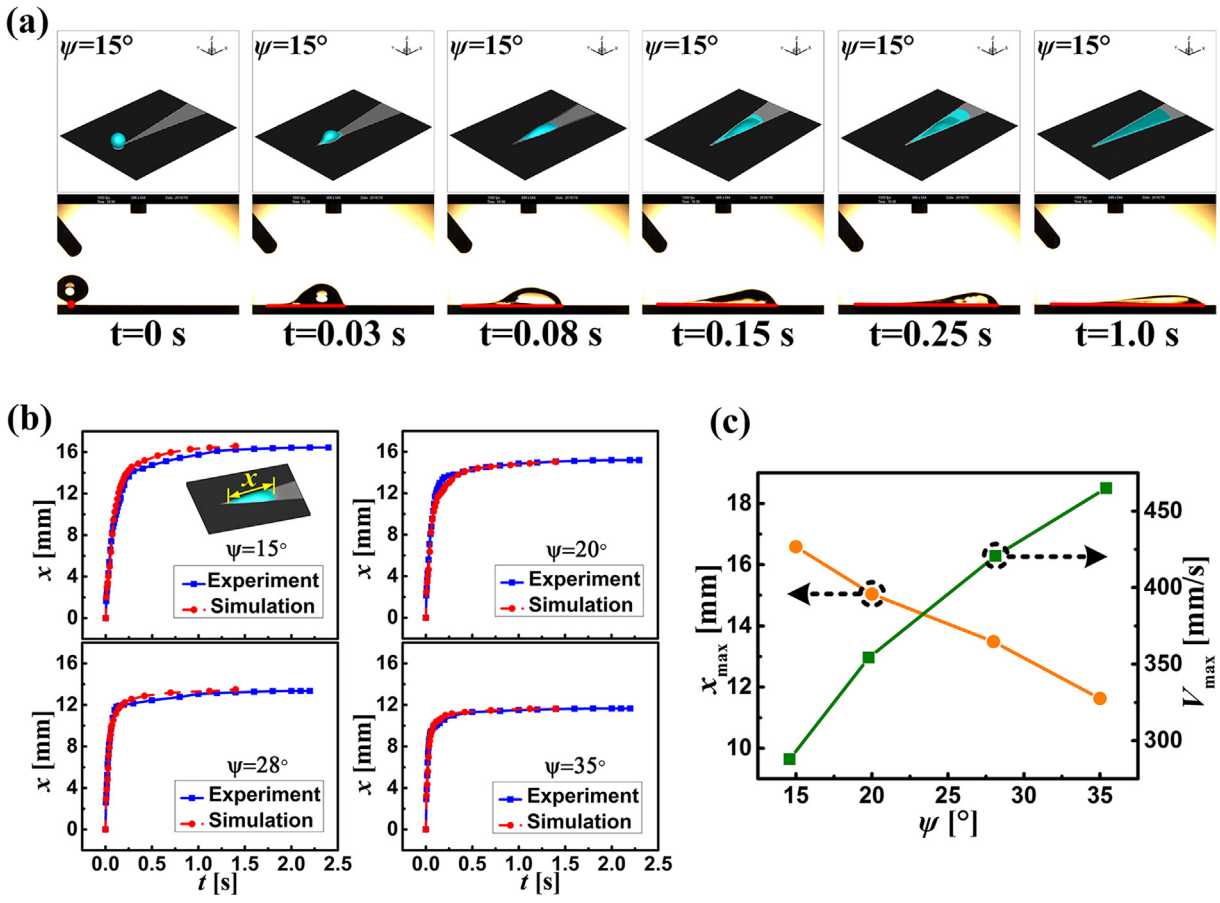

Fig. 2. (a) Comparison of the simulated results and snapshots. (b) Comparison of droplet move distance x as a function of time t in the experiments and simulations. (c) Final droplet move distance x_{max} and maximum velocity V_{max} as a function of vertex angle ψ in the simulations.

As shown in the set-up graph of Fig. 1(a), inside the wedge-shaped region is hydrophilic as well as the outside region is hydrophobic. In the computational domain of 240 × 200 × 50 lattices, a spherical water droplet of radius r = 16 lattices was placed on the tip of a hydrophilic wedge-shaped region. The static contact angles of hydrophilic and hydrophobic regions were set as θ_{phi} = 25°, θ_{pho} = 145°. The periodical boundary condition was used in the horizontal sides of the lattice, while the "bounce-back" was used at the patterned surface [19]. The initial density ratio ($\lambda = \rho_{liquid}/\rho_{air}$) will greatly influence the spreading dynamics. To determine feasible initial densities, we simulated water droplet spreading on a 15° vertex angle wedge-shaped patter surface with different λ, and the results of spreading morphology are shown in Fig. 1(b). For λ from 1 to 9.8, the phase separation is diverging. For λ from 9.8 to 28.4, it shows that the phase separation is partly unstable. For λ from 28.4 to 50.5, it can be seen that the phase separation is very stable, which is accurate to reflect the droplet morphology evolution during the spreading process. However, a too large λ will induce a too small cohesion force, which leads to the diffusion of liquid phase (it can be seen that the liquid spreads to the hydrophobic region instead of the hydrophilic region). Therefore, we chose λ = 33.3 (ρ_{liquid} equals 2.00 and ρ_{air} equals 0.06) in our simulation. To relate the dimensionless simulation parameters with real physical quantities, length, time and mass scales ($L_0 = 1.55 \times 10^{-4}$ m, $T_0 = 1.4 \times 10^{-5}$ s, $M_0 = 1.5 \times 10^{-9}$ kg) are required. A simulation parameter will convert to a real physical quantity after being multiplied by $[L_0]^{n_1}[T_0]^{n_2}[M_0]^{n_3}$. Here we simulated four cases with various vertex angles (ψ = 15°, 20°, 28°, 35°) of wedge-shaped pattern.

3. Experiments

To validate the results of LBM, we deposited a 100–200 nm Al film on a 5 × 5 × 1 mm copper substrate through an e-beam evaporation coating machine (Alpha. Plus, EB-500S), followed by oxygen plasma treatment (Harrick, PDC-002-HP, 29.6 W) and 1H, 1H, 2H, 2H-perfluorodecanethiol (HDFT) modification [20]. The contact angle of 25° was achieved on the hydrophilic Al region, while the contact angle of 145° was obtained on the hydrophobic Cu region. After then, the experiment of a 20 μl water droplet spreading on the fabricated surface were captured by a high speed camera (Photron Fastcam SA3) at the frame rate of 1000 fps. More details can be referred to Ref. [14].

4. Results and discussions

The simulated results and snapshots of a water droplet spreading on a wedge-shaped pattern surface with the vertex angle of 15° are shown in Fig. 2(a), which indicates the similarity of spreading results in both the LBM and experiment. Firstly, the droplet spontaneously spreads from the hydrophobic region to hydrophilic region driven by the difference of adhesive force between two regions. After that, the whole droplet further spreads forward. The phenomena observed in other three cases are similar to that

Table 1
Deviation of move distance between the simulations and experiments.

Case		Deviation			
		$N_{t,\max}$	$N_{t,\min}$	$N_{t,\text{average}}$	S
I	$\psi = 15°$	12.16%	1.62%	6.11%	3.14%
II	$\psi = 20°$	17.25%	0.04%	4.53%	4.39%
III	$\psi = 28°$	18.78%	0.38%	4.73%	4.12%
IV	$\psi = 35°$	20.75%	0.03%	4.18%	5.33%

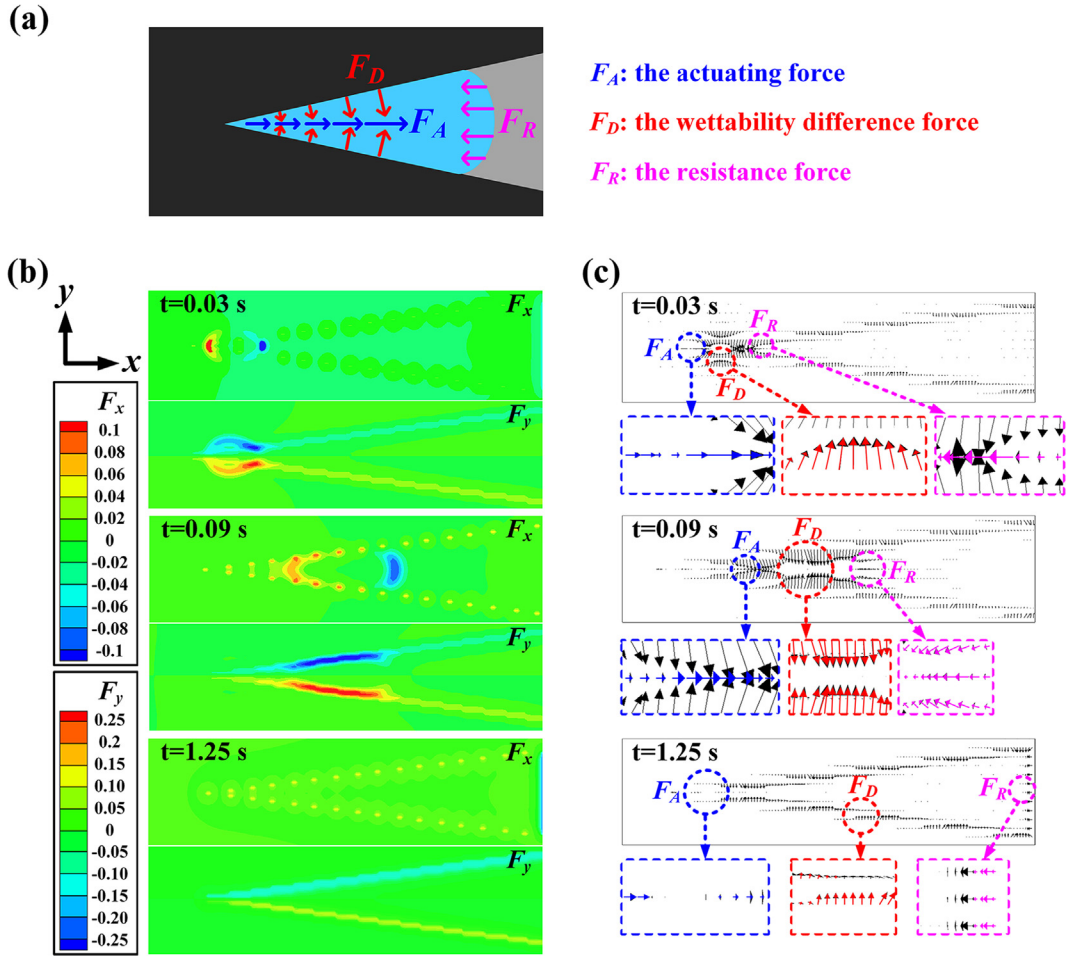

Fig. 3. (a) Analyses of forces acting on a droplet. (b) Simulated force contours and (c) force vectors in the 15° vertex angle case at time of t = 0.03 s, 0.09 s and 1.25 s.

in the 15° case. We further qualitatively characterize the move distance x (shown as the inset picture in Fig. 2(b)) of water droplet. Fig. 2(b) shows the x-t curves in four cases (ψ = 15°, 20°, 28°, 35°), in which red lines represent the converted simulated results and the blue[1] lines represent the experimental results. By further analyzing Fig. 2(b), we obtained the simulated final move distance ($x_{\max}$) and the maximum velocity ($V_{\max}$) and drew the $x_{\max}$-ψ curve and the $V_{\max}$-ψ curve in Fig. 2(c) to analyze the impact of vertex angle ψ. It is obvious that the final move distance of droplet decreases with the increase of vertex angle, while the maximum velocity increases.

To discuss the accuracy of the LB model in detail, deviations of x between the simulations and experiments at each moment were calculated. The deviation N_t is defined as the ratio of $x_{e,t}$–$x_{s,t}$ to $x_{e,t}$, where $x_{e,t}$ represents the x measured in the experiments and $x_{s,t}$ is the x obtained from the simulations. The maximum deviations in four cases are 12.16%, 17.25%, 18.78%, 20.75%, respectively. The standard deviation of N_t is defined as:

$$S = \sqrt{\frac{\left(N_{t,i} - \overline{N_t}\right)^2}{n-1}} \tag{9}$$

The results are summarized in Table 1. The average deviations in four cases are 6.11%, 4.53%, 4.73% and 4.18%, and the standard deviations are 3.14%, 4.39%, 4.12%, 5.33%. Overall, the results indicate the accuracy of the LB model for such spreading process.

To further discuss the driving mechanism, we analyzed the forces acting on droplet. As shown in Fig. 3(a), the forces effecting the spreading dynamics of droplet mainly include three kinds of forces: the actuating force (F_A), the wettability difference force (F_D), the resistance force (F_R). Obviously, the droplet spreads forward under the driving forces of F_A and F_D, and F_R is the opposite force hindering the spread motion. To validate the force analysis,

[1] For interpretation of color in Fig. 2, the reader is referred to the web version of this article.

we calculated and obtained the forces acting on water droplet in the simulation of 15° vertex angle case. Fig. 3(b) demonstrates the contours of F_x (the projected value of F on x direction) and F_y (the projected value of F on y direction) at t = 0.03 s, 0.09 s, 1.25 s. In F_x contour, the forces exerting on the end of the liquid promote the spread forward, while the forces exerting on the front of the liquid hinder it. Besides, the forces along the edge of the wedge-shaped pattern is positive, from which we can consider them as promotional roles to the spreading process. In F_y contour, it is obvious that the forces along the edge of the wedge-shaped pattern exert from the hydrophobic region to the hydrophilic region, which reveals the wettability difference makes water droplet spreading only along the hydrophilic wedge-shaped pattern. After then, we analyzed the force vectors at time of t = 0.03 s, 0.09 s, 1.25 s in Fig. 3(c), in which the forces can be divided into F_A, F_D, F_R (shown as locally enlarged views in each force vector). Overall, the force analyses in the contour and vector are consistent with that in Fig. 3(a).

5. Conclusion

In this study, we have investigated water droplets' spontaneously spreading phenomenon on wedge-shaped pattern surface with various vertex angles (ψ = 15°, 20°, 28°, 35°) by both the LBM and experiments. The move distances of water droplets were characterized in both the simulations and experiments with the average deviation within 6.11%. The final move distance of droplet decreases with the increase of vertex angle, while the maximum velocity increases. To discuss the driving mechanism in the spreading process, the forces acting on droplet are divided into F_A, F_D, F_R followed by simulated validation via the force contour and vector. The proposed LB model is found to be an effective approach to explore the driving mechanism to better tune and control the directional spreading of the surface tension-driven droplet.

Conflict of interest

There are no conflicts of interest.

Acknowledgments

The authors would like to acknowledge the financial support by National Natural Science Foundation of China (51625601, 51576078, and 51606074), the Ministry of Science and Technology of the People's Republic of China (Project No. 2017YFE0100600), the Financial support from Creative Research Groups Funding of Hubei Province (2018CFA001).

References

[1] L. Zhang, Y.F. Zhang, Research on energy saving potential for dedicated ventilation systems based on heat recovery technology, Energies 7 (7) (2014) 4261–4280.
[2] B. Shang, Y. Ma, R. Hu, et al., Passive thermal management system for downhole electronics in harsh thermal environments, Appl. Therm. Eng. 118 (2017) 593–599.
[3] X.B. Luo, R. Hu, S. Liu, K. Wang, Heat and fluid flow in high-power LED packaging and applications, Prog. Energy Combust. Sci. 56 (2016) 1–32.
[4] Y.P. Ma, W. Lan, B. Xie, et al., An optical-thermal model for laser-excited remote phosphor with thermal quenching, Int. J. Heat Mass Transf. 116 (2018) 694–702.
[5] C. Yuan, L. Li, B. Duan, B. Xie, Y.M. Zhu, X.B. Luo, Locally reinforced polymer-based composites for efficient heat dissipation of local heat source, Int. J. Therm. Sci. 102 (2016) 202–209.
[6] C. Yuan, B. Xie, M.Y. Huang, R.K. Wu, X.B. Luo, Thermal conductivity enhancement of platelets aligned composites with volume fraction from 10% to 20%, Int. J. Heat. Mass. Transf. 94 (2016) 20–28.
[7] Y.P. Ma, R. Hu, X.J. Yu, W.C. Shu, X.B. Luo, A modified bidirectional thermal resistance model for junction and phosphor temperature estimation in phosphor-converted light-emitting diodes, Int. J. Heat. Mass. Transf. 106 (2017) 1–6.
[8] J.W. Rose, Dropwise condensation theory and experiment: a review, Proc. Imeche Part A2 J. Power Energy 216 (2) (2005) 115–128.
[9] E.K. Her, T.J. Ko, K.R. Lee, et al., Bioinspired steel surfaces with extreme wettability contrast, Nanoscale 4 (9) (2012) 2900.
[10] H.S. Khoo, F.G. Tseng, Spontaneous high-speed transport of subnanoliter water droplet on gradient nanotextured surfaces, Appl. Phys. Lett. 95 (6) (2009) 5556.
[11] E.S. Kooij, H.P. Jansen, O. Bliznyuk, et al., Directional wetting on chemically patterned substrates, Colloids Surf., A 413 (21) (2012) 328–333.
[12] S. Deng, W. Shang, S. Feng, et al., Controlled droplet transport to target on a high adhesion surface with multi-gradients, Sci. Rep. 7 (2017) 45687.
[13] A.K. Das, P.K. Das, Schemes for the fragmentation and merging of droplets resting on a solid substrate using a patterned wettability gradient, Langmuir Acs J. Surf. Colloids 26 (20) (2010) 15883.
[14] M.H. Alheshibri, N.G. Rogers, A.D. Sommers, et al., Spontaneous movement of water droplets on patterned Cu and Al surfaces with wedge-shaped gradients, Appl. Phys. Lett. 102 (17) (2013) 146–151.
[15] G.H. Tang, H.H. Xia, Y. Shi, Study of wetting and spontaneous motion of droplets on microstructured surfaces with the lattice Boltzmann method, J. Appl. Phys. 117 (24) (2015).
[16] A. Montessori, P. Prestininzi, M. La Rocca, et al., Entropic lattice pseudo-potentials for multiphase flow simulations at high Weber and Reynolds numbers, Phys. Fluids 29 (9) (2017) 092103.
[17] A. Montessori, G. Falcucci, M.L. Rocca, et al., Three-dimensional lattice pseudo-potentials for multiphase flow simulations at high density ratios, J. Stat. Phys. 161 (6) (2015) 1404–1419.
[18] X. Shan, H. Chen, Simulation of nonideal gases and gas–liquid phase transitions by the lattice Boltzmann equation, Phys. Rev. E 49 (4) (1994) 2941–2948.
[19] H. Huang, D.T. Thorne, M.G. Schaap, M.C. Sukop, Proposed approximation for contact angles in Shan-and-Chen-type multicomponent multiphase lattice Boltzmann models, Phys. Rev. E 76 (2007) 066701.
[20] C. Yuan, M.Y. Huang, X.J. Yu, Y.P. Ma, X.B. Luo, A simple approach to fabricate the rose petal-like hierarchical surfaces for droplet transportation, Appl. Surf. Sci. 385 (2016) 562–568.